Pharmaceutica Analytica Acta

Majolino eta al., Pharm Anal Acta 2015, 6:4
http://dx.doi.org/10.4172/2153-2435.1000356

Research Article Open Access

Relationship between Elastic Properties and Gel-to-Sol Transition in Cyclodextrin-Based Hydrogel

Majolino D[1*], Venuti V, Crupi V[1], Rossi B, Fontana A[3], Mele A , Melone L[4], Punta C[4], Trotta F , Giarola M and Mariotto G[7]

[1]Department of Physics and Earth Sciences, University of Messina, Viale Ferdinando Stagno D'Alcontres, Messina, Italy
[2]Elettra - Sincrotrone Trieste, Strada Statale, Area Science Park, Trieste, Italy
[3]Department of Physics, University of Trento, Via Sommarive, Povo, Trento, Italy
[4]Department of Chemistry, Materials and Chemical Engineering "G. Natta", Politecnico di Milano, Piazza L. da Vinci, Milano, Italy
[5]INSTM Local Unit, Politecnico di Milano, Milano, Italy
[6]Department of Chemistry, University of Torino, Via Pietro Giuri, Torino, Italy
[7]Department of Computer Science, University of Verona, Strada le Grazie, Verona, Italy

Abstract

In order to elucidate the effects of the nature of the cross-linker, of the hydration level and of the hydrophobic/hydrophilic balance on the macro- and microscopic properties of a paradigmatic model of polysaccharide hydrogel, an integrated approach based on the combined use of low-frequency Raman scattering and FTIR-ATR absorption has been developed. The proposed methodology aims to explore the stability range of the liquid and gel phase diagram of the system. This approach was applied to cyclodextrin based nanosponges (CDNS), prepared by polymerization of α-, β-, and γ-cylcodextrins (CDNS) with an activated derivative of ethylenediamine tetra acetic acid. It revealed successful, on one side, for a comparative analysis of the elasticity, as mesoscopic parameter, of the dry polymeric network, measured by Raman spectroscopy in the low frequency (0 ÷ 150 cm^{-1}) range, and, on the other side, for the investigation of the water holding capacity, as macroscopic parameter, through the analysis of the vibrational dynamics of water molecules in the swollen polymers, monitored by FTIR-ATR spectroscopy in two selected wavenumber regions, i.e. 2800 ÷ 3800 cm^{-1} and 1500 ÷ 1800 cm^{-1}, where the O-H stretching and H-O-H bending

vibrations respectively occur. As main result, the same evolution as a function of the molar ratio *n*, has been observed for the elasticity on mesoscopic scale, as described by the Boson Peak (ω_{BP}) and the swelling ability on macroscopic scale, expressed by the mass ratio *m* describing the gel-to-sol transition in these systems. From the results, the way for a rational development of stimuli-responsive systems with specific performances, by modulating the stability range of the liquid suspension and gel phases properly changing the molar ratio *n* during the synthesis, is opened.

Keywords: Cyclodexrin-based hydrogel; FTIR-ATR spectroscopy; Raman spectroscopy; Swelling

Introduction

Cyclodextrin nanosponges (CDNS) are hyper-cross-linked polymers obtained by polycondensation between α-, β-, or γ-cyclodextrins (α-, β-,or γ-CD) and suitable cross-linking agents (CL), such as carbonyldiimidazole (CDI) [1,2], pyromellitic anhydride (PMA) [1] or activated derivatives of ethylenediamine tetra acetic acid (EDTA) [3,4]. The reaction leads to the formation of a three-dimensional sponge-like structure, whose main functional features are the presence of both hydrophilic and hydrophobic cavities in the polymeric network, and the possibility to modulate the molecular architecture of the system by a careful choice of the polymerization conditions [5].

CDNS are biocompatible material with negligible toxicity on cell cultures and well-tolerated after injection in mice, as recently demonstrated by in vivo studies [5,6]. Recently, the drug delivery capabilities of these polymeric matrices have been widely investigated and recently reviewed [5,7-11]. These studies revealed that CDNS can encapsulate either lipophilic or hydrophilic active pharmaceutical ingredients, protect them against undesired degradation, enhance water solubility when necessary, facilitate their gradual release over extended times [12], thus increasing the bioavailability at the target site. More interestingly, cyclodextrin nanosponges showed superior inclusion ability with respect to native cyclodextrins (CD) and they seem to be good candidates as efficient capture/delivery systems for a large class of organic and inorganic compounds. In particular, the design of these new nanocarriers as a strategy for the delivery of anti-cancer drugs offers a potential platform to overcome some limitations of current clinical treatments and to achieve targeted release into tumour tissues [13].

In addition, CDNS have been proved to play a fundamental role in the rational design of new soft materials for application in agriculture [14] and environmental control [15]. Finally, the chirality of the CDNS components was recently exploited as chiral reaction environment for photochemical asymmetric synthesis showing a surprising capability of asymmetric induction [16,17].

By the combined use of many experimental techniques [1-4], such as inelastic light scattering, nuclear magnetic resonance and Fourier transform infrared absorption in attenuated total reflectance geometry (FTIR-ATR), we recently demonstrated that the cross-linking degree

***Corresponding author:** Majolino D, Department of Physics and Earth Sciences, University of Messina, Viale Ferdinando Stagno D'Alcontres, Messina, Italy, Tel: +390906765237; Fax: +39090395004; E-mail: majolino@unime.it

Received February 25, 2015; **Accepted** March 31, 2015; **Published** April 07, 2015

Citation: Majolino D, Venuti V, Crupi V, Rossi B, Fontana A et al. (2015) Relationship between Elastic Properties and Gel-to-Sol Transition in Cyclodextrin-Based Hydrogel. Pharm Anal Acta 6: 356. doi:10.4172/2153-2435.1000356

and the elastic properties of CDNS are strongly dependent on the chemical structure of the cross-linking agent and on the relative amount of the cross-linker with respect to the monomer CD (i.e. *n* = cross-linking agent/CD molar ratio) used during the synthesis of the polymers. In particular, in the case of ester-bridged CDNS, a triggering of stiffness and connectivity has been always observed at n = 6, revealing that a six-fold excess of CL with respect to CD corresponds to a balance between two competing processes , i.e. reticulation and branching of CD units [1,3,4].

Although some types of CDNS are shown to be insoluble in water and in other organic solvents [5], ester-bridged CDNS [1,3,4] exhibit a marked swelling behaviour. Indeed, the formation of highly viscous, gel-like dispersion, similarly to hydrogels [16,17] is often observed when contacting CDNS with aqueous solution. The ability to absorb water – up to 40 times their dry weight – is particularly interesting in view of the application of CDNS as efficient water nano-containers. Thanks to this intriguing properties, and in addition to the relative low cost of production of CDNS, low-toxicity to humans and biodegradability, these soft materials are potential new members of the tool-case of polymeric host systems for high value and high social impact applications, such as tissue engineering and regenerative medicine [18,19]. In these latter fields, hydrogels have been often used as localized drug depots [20-22], since they are hydrophilic and biocompatible and their drug release rates can be triggered [23] by interactions with biomolecular stimuli [24,25]. Additionally, thixotropic hydrogels allow both injectability and local persistence of gel once placed in situ. Remarkable applications for cartilage, central nervous system, and spinal cord injury repair strategies based on hydrogel scaffolds have been also reported [25,26]. In this scenario, the possibility mentioned above of tuning the swelling, the cross-linking density and the degradation rate of CDNS based hydrogels opens the possibility to engineer the release kinetic profile of these systems in order to achieve a desired drug release schedule.

The structural and dynamic characterization of CDNS hydrogels is still a challenging task in soft-matter physical chemistry, because thorough knowledge of these innovative materials at molecular level is still an ambitious objective to be reached due to the complex molecular architecture of the system under investigation and the lack of crystallinity often observed. The control of the most important structural and dynamic features of CDNS during their synthesis is a pivotal objective of our research line, with the long term target of designing new smart hydrogel with tunable inclusion/release properties. This, in principle, can be achieved by designing stimuli-responsive CDNS hydrogels. As an example, CDNS able to modify their structural properties or to undergo phase transition in a controlled way, e.g. by changing temperature and/or pH, should fulfill the requirements for entrapment and release of bio-active compounds. In this sense, we recently provided experimental evidence that CDNS hydrogels can undergo rigid-gel to liquid-suspension phase transitions when the hydration level of the system was progressively increased [27-29]. These phase transitions of the hydrogel have been correlated with the evolution of FTIR-ATR and Raman scattering experimental parameters [27-30], with the aim of understanding basis of the gel-to-sol transition observed in CDNS hydrogel at molecular level.

The entire collection of experimental results suggested that the macroscopic properties of the gel phase, such as the water holding capacity and the rigidity of the gel network, are closely related to the complex interplay of physical and covalent bonds over different length-scale to yield the formation and stabilization of the hydrogel network. As main result of the vibrational analysis, a characteristic cross-over hydration level (i.e. h_{cross} defined as weight ratio H_2O/CDNS used in the preparation of the hydrogel) was observed for all the CDNS hydrogel investigated. This point identifies a significant change in the cooperativity pattern of the water molecules confined in the hydrophilic pores of CDNS polymer. Indeed, the tetrahedral connectivity pattern of H_2O becomes favored with respect to the no bulk-like arrangements of the water molecules for $h>h_{cross}$. More interestingly, the cross-over hydration level seems to match also with the value of hydration above which the system evolves from a rigid gel state to a fluid suspension [27-29]. Moreover, recent studies suggested that the value of h_{cross} estimated for some type of CDNS hydrogel may be dependent on the molar ratio *n* and on the type of cyclodextrin used in the polymer synthesis [28].

Based on a review of these aforementioned results, improved by the collection of new data, we present here a detailed investigation of the phase diagram of α-, β-, and γ-CD nanosponge hydrogels, using the values of h_{cross} measured via FTIR-ATR as suitable descriptor of the water holding capacity at macroscopic level. The changes observed in the cross-over hydration level as a function of the molar ratio *n*, are strictly connected to the evolution of the elastic modulus of the polymeric material which are preliminarily described in dry state, over the mesoscopic length scale, by the behavior of the low-frequency vibrational modes of the system as explored by Raman technique.

The entire amount of the obtained results provide data useful for the assessment of the role played by the chemical structure of cross-linking agent, the water content and the starting carbohydrate monomer in defining the overall properties of nanosponge hydrogel. This is a good starting point for the modulation of the stability range of the liquid suspension and gel phases, with remarkable perspectives in the design of suitable stimuli-responsive systems.

Materials and Methods

Materials

The nanosponges were obtained following the synthetic procedure previously reported [31,32]. In the present study, ethylenediamine tetra acetic acid (EDTA) dianhydride was used as cross-linking agent. Anhydrous α- and γ-cyclodextrin (α-CD, γ-CD) were dissolved at room temperature in anhydrous DMSO containing anhydrous Et3N. Then, the cross-linking agent EDTA dianhydride was added at 1:*n* molar ratios (with *n* = 2, 4, 6, 8, 10) under intense magnetic stirring. The polymerization was complete in few minutes obtaining a solid that was broken up with a spatula and washed with acetone in a Soxhlet apparatus for 24h. The pale yellow solid was finally dried under vacuum.

The corresponding hydrogel of CDNS were prepared by adding to the dry samples suitable amount of double-distilled water (Sigma) in order to obtain different levels of hydration *h* in the range 2 ÷ 25.5. The hydration level *h* is defined as weight ratio H_2O/CDNS.

Methods

Low-frequency Raman scattering measurements: Low-frequency Raman spectra were carried out at room temperature in back-scattering configuration on dry α- and γ-CDEDTA1*n* (*n* = 2, 4, 6, 8, 10) nanosponges deposited on a glass slide (the data relative to the other samples and reported here are taken from References [3,4]).

Cross-polarized spectra were recorded over the wavenumber range between 3.5 and 400 cm^{-1} by using a triple-monochromator spectrometer (Horiba-Jobin Yvon, model T64000) set in double-subtractive/single configuration and equipped with holographic grating

1800 grooves/mm. Micro-Raman spectra were excited by the 647.1 nm wavelength of an argon/krypton ion laser and detected by a CCD detector cryogenically cooled by liquid nitrogen. Exciting radiation was focused onto the sample surface with a spot size of about 1 m^2 through a 80X objective with NA = 0.75. The resolution was about 0.36 cm^{-1}/pixel. No appreciable damage due to possible heating of the sample was observed as resulting from an accurate inspection of the irradiated sample surface throughout the camera coupled to the microscope objective and carried out after each measurement. Moreover, four Raman spectra were recorded from different regions of each examined sample in order to verify their reproducibility.

FTIR-ATR measurements: FTIR-ATR measurements were performed, at room temperature, on α-CDEDTA1*n* (*n* = 4, 8) and γ-CDEDTA1*n* (*n* = 2, 4, 6, 8, 10) hydrogels (the data relative to the other samples and reported here are taken from References [27,28]), prepared, as previously described, by hydration in water of the corresponding dry samples of CDNS. The spectra were collected by a Bomem DA8 Fourier transform spectrometer, exploiting a Globar source, in combination with a KBr beamsplitter, a DTGS/KBr detector. Spectra were collected in the 400 ÷ 4000 cm^{-1} wavenumber range. The samples were contained in Golden Gate diamond ATR system, just based on the ATR technique [33-35]. The spectra were recorded in dry atmosphere, in order to avoid dirty contributions, with a resolution of 4 cm^{-1}, automatically adding 100 repetitive scans in order to obtain a good signal-to-noise ratio and high reproducibility. All the IR spectra were normalized for taking into account the effective number of absorbers. No mathematical correction (e.g., smoothing) was done, and spectroscopic manipulation such as baseline adjustment and normalization were performed using the Spectracalc software package GRAMS (Galactic Industries, Salem, NH, USA). For the O–H stretching region (2800 ÷ 3800 cm^{-1}), second derivative computations have been used for evaluating the wavenumbers of the maxima of the different sub-bands. Multiple curve fitting into Voigt profiles were then applied to the experimental profiles based on these wavenumber values, by using the routine provided in the Peak Fit 4.0 software package. The statistical parameters defined in the software manual were used as a guide to best-fit and allowed to vary upon iteration until converging solution was reached. The best-fit was characterized by $r^2 \approx 0.9999$ for all the investigated systems.

Results and Discussion

Following the considerations done in the introduction, two main interconnected aspects will be presented and discussed here: the analysis, on one side, of the elastic properties at mesoscopic level of the dry polymeric network, and, on the other side, the study of the vibrational dynamics of water molecules in the swollen polymers, focusing on the evolution of the characteristic cross-over hydration level as key-parameter for describing the water holding capacity of these systems at macroscopic scale. The main investigating tools are, in the order, the Raman spectra collected at low frequency (0 ÷ 150 cm^{-1}) for the dry systems, and the FTIR-ATR spectra in selected frequency windows, 2800 ÷ 3800 cm^{-1} and 1500 ÷ 1800 cm^{-1}, for the corresponding hydrogels.

Dry state

Starting from the analysis of Raman intensity in the low frequency domain, the spectra reported in Figures 1a and 1b show, as an example, the low-frequency range (0 ÷ 150 cm^{-1}) of the cross-polarized Raman intensity obtained from dry samples of α-CDNSEDTA1*n* (*n* = 2, 4, 6) and γ-CDNSEDTA1*n* (*n* = 2, 8).

This spectral region is characterized by the presence of the boson peak (BP), a peculiar vibrational feature observed in the inelastic light and neutron scattering spectra of disordered systems [36,37]. Although the origin of these low-frequency vibrational modes is still subject of debate, it was experimentally proved that the frequency position and the intensity of BP are strongly correlated to the transformation of the elastic properties of the system over a mesoscopic length scale. In particular, it was reported that the position of the maximum of BP tends to move to higher energies when the stiffness of the material increases, considering both inorganic [38] and organic [39] amorphous systems. On the basis of these findings, we propose that the spectral features of the BP observed in the case of CDNS can be used as qualitative descriptors of the elasticity of the CDNS polymeric network [1,3,4,40].

The existence of a scaling law for the BP evolution, which reflects the relative modifications of the elastic properties of the CDNS polymers, was recently assessed by comparison with the density of vibrational states of the same systems derived from inelastic neutron scattering experiments [40]. Finally, in the case of CDNS based on pyromellitic anhydride (PMA) and carbonate cross-linking (CDI), the modifications observed in the frequency position of BP for different types of CDNS were found to correlate with the trend observed for the Brillouin sound velocity measured on the same samples [1]. At this stage it is worth reminding the physical interpretation of such properties: indeed, BP and the Brillouin peak are both related to the elastic constants of the system under exam, the former on an interatomic distances length-scale, the latter on a wider scale, extending up to hundreds of nanometers.

The data reported in Figure 1 show significant changes in the position and intensity of BP with increasing n in the case of α-CDEDTA1*n* (Figure 1a), whereas the evolution of BP appears much less evident for γ-CDEDTA1*n* (Figure 1b).

In order to obtain a quantitative estimation of the BP position, the vibrational component was isolated by subtracting from the total experimental profiles of Figure 1 the quasi elastic (QE) contribution, which appears as a broadening of the elastic line superimposed to the BP. A well-assessed fitting procedure [1,3,4,39,41] was applied for the data handling. Accordingly, the total Raman scattering intensity $I_{Raman}(\omega)$ can be satisfactorily reproduced by the sum of the QE signal – modelled by a Lorentzian function centred at zero wavenumber with width Γ and amplitude A – and the BP, accounting for the pure vibrational dynamics. The peak shape and position of its maximum, ω_{BP}, are reproduced by a Log-normal distribution function with width W and amplitude B (equation 1).

$$I_{Raman}(\omega) = \frac{A\Gamma}{\Gamma^2 + \omega^2} + B\exp\left\{-\frac{\left[\ln\left(\frac{\omega}{\omega_{BP}}\right)\right]^2}{2W^2}\right\} \quad (1)$$

A typical example of the best fitting results is reported in Figure 1c for α-CDEDTA12 nanosponge, where the two different components of the Raman spectra are evidenced.

In Figure 2a the Raman spectra of α-CDEDTA1*n* nanosponges (*n* = 2, 4, 6, 8, 10) are shown after subtraction of the QE contribution in the energy range 0 ÷ 150 cm^{-1}.

It is noteworthy to remark that the subtraction of the QE signal from the experimental spectra does not substantially modify the overall trend of the BP component already observed in the raw data of Figures 1a and 1b.

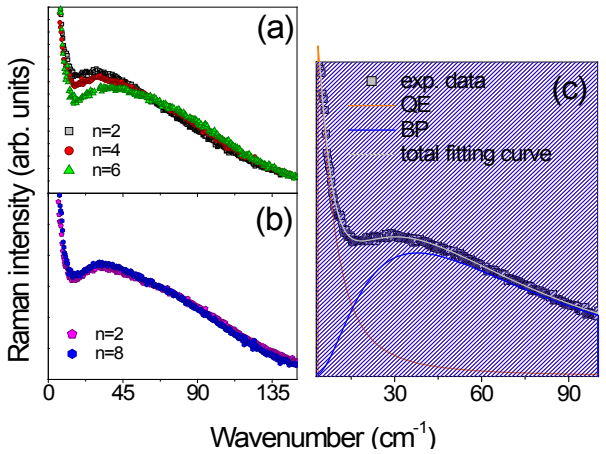

Figure 1: Cross-polarized Raman intensity of dry samples of α-CDEDTA1n (*n* = 2, 4, 6) (a) and γ-CDEDTA1n (*n* = 2, 8) (b) nanosponges in the low-frequency range 0 ÷ 150 cm-1. (c) Typical example of the best fitting results for α-CDED-TA12: the experimental data (grey squares) are reported together with the total fitting curve and the different components (QE, quasi-elastic; BP, boson peak).

A clear evolution of the wavenumber and intensity of maximum of the BP as a function of molar ratio *n* is pointed out in Figure 2a. In particular, on passing from *n* = 2 to *n* = 6, ω_{BP} shifts towards higher frequencies, and in the meanwhile its intensity decreases. Conversely, for molar ratios going from 6 to 10, the opposite trend is observed. These results give evidence that α-CDNSEDTA1*n* shows the same *n*-dependence for the stiffness of the polymeric network reported in previous papers in the case of β-CD-nanosponges synthesized by other types of cross-linkers [1,3,4]. As evident in the spectra of Figure 2a, two opposite trends can be observed. The cross-linking increases reaching a maximum for *n* = 6. This critical value seems to be the result of an ideal balance between activated carboxylic groups and free hydroxyl functions onto the cyclodextrin units, leading to the highest interconnectivity between α-CD cavitands (Scheme 1).

For *n* > 6, an excessive EDTA grafting on each CD unit prevents enhanced cross-linking of the polymer and a branching of CD units takes probably place, whose conformational degrees of freedom result in a general decreasing of the stiffness of the material [1]. It should be pointed out that the change of the BP intensity observed in the spectra of Figure 2 is only an apparent effect due to its frequency shift with the molar ratio *n* [42].

In Figure 2b the observed frequency position of the boson peak ω_{BP} is plotted as a function of the parameter *n* for α-CDEDTA1*n* and γ-CDEDTA1*n* nanosponges (hexagons and triangles in Figure 2(b), respectively). This representation illustrates more clearly the two behaviors mentioned before and the critical value for *n* = 6 in the case of α-CDEDTA1*n*. Conversely, a less defined trend, if any, can be worked out for γ-CDEDTA1*n* . In this case, the higher cavitand dimension for -CD, which corresponds to an enhanced steric hindrance, limits the possibility to modulate the cross-linking degree by varying the CD/EDTA ratio. In fact, the maximum of interconnectivity is already reached for low values of *n*.

Hydrated state

The nanosponges were hydrated to form hydrogels with a known amount of water (see Materials and Methods section for the definition of the hydration level *h*).

Figures 3a-3c reports, as an example, the FTIR-ATR spectra, in the 2800 ÷ 3800 cm^{-1} wavenumber range, of γ-CDEDTA1*n* (*n* = 2, 6, 10) hydrogel at increasing values of hydration level *h*. For a better comparison of the data, the spectra have been normalized to the total area.

In such spectral window the infrared bands assigned to the O-H stretching vibrations of water are typically observed. As well known [43-45], the O-H stretching vibration gives fundamental information on the hydrogen bonding scheme developed by H_2O molecules present in the system.

The data of Figure 3 show an enhancement of the intensity of the low-frequency shoulder of the O-H stretching profile with increasing hydration level *h*. These spectral modifications with increasing water content are consistent with the enhancement of the cooperative nature of the intermolecular hydrogen-bond (HB) network of water molecules. Indeed, after the binding sites on the polymeric backbone have been saturated of water molecules, the excess water tends to interconnect in tetrahedral, bulk-like structures.

The information extracted by the analysis of the O-H stretching vibration can be corroborated by those provided by the inspection of the H-O-H bending vibration of water in the 1500 ÷ 1800 cm^{-1} range. The behaviour observed for HOH bending mode in bulk water [46] gave indication that the HOH bending mode is hardly sensitive to the different levels of connectivity of hydrogen bond patterns developed by H_2O, and suggested the interpretation that the bending band mostly reflects the population of water molecules that do not lie in a symmetric tetrahedral environment.

The FTIR-ATR spectra recorded in the 1500 ÷ 1800 cm^{-1} wavenumber range for α- and γ-CDEDTA14 hydrogels at *h* = 3.0 and 21.5 are shown in Figure 4, as examples.

All the experimental profiles clearly show two different features, a broad band centered at ~1630 cm^{-1} and assigned to the H-O-H bending vibration, and a contribution at ~ 1730 cm^{-1}, corresponding to C=O

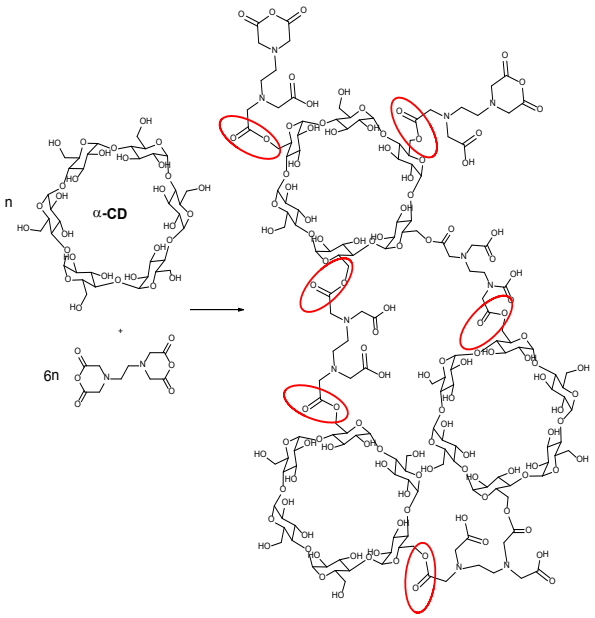

Scheme 1: Cross-linking of α-CD in the presence of activated EDTA

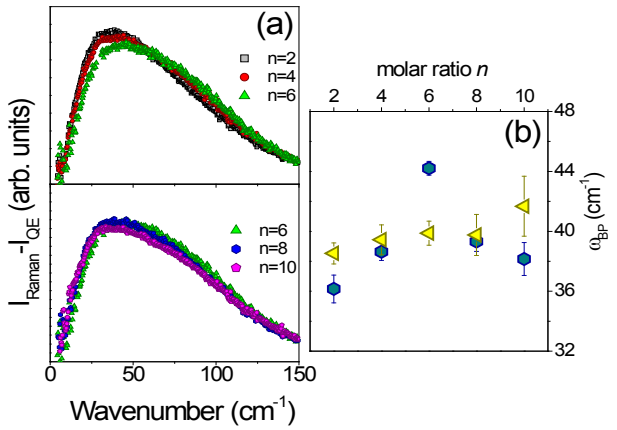

Figure 2: (a) Raman spectra of dry samples of α-CDEDTA1*n* nanosponges (*n* = 2,4,6,8,10) after subtraction of the QE contribution in the energy range 0 ÷ 150 cm^{-1}. (b) Estimated frequency position of the boson peak ω_{BP} as a function of the parameter n for α-CDEDTA1*n* (cyan hexagons) and γ-CDEDTA1*n* (yellow triangles) nanosponges.

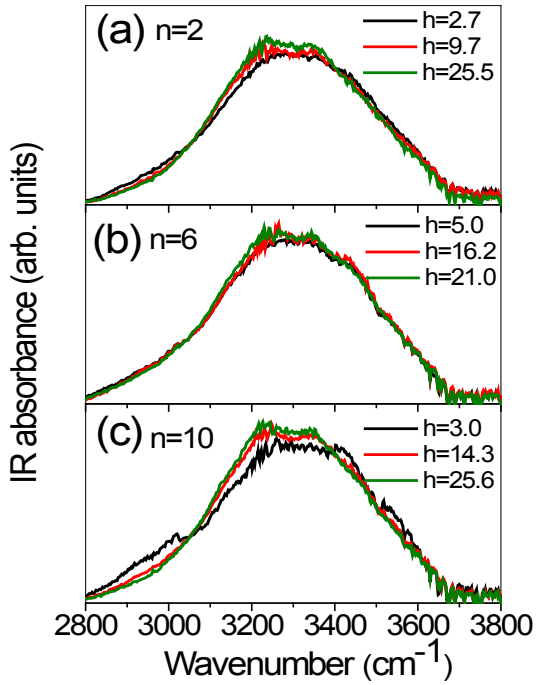

Figure 3: Examples of FTIR-ATR spectra of γ-CDEDTA1*n* (*n* = 2, 6, 10) hydrogels in the 2800 ÷ 3800 cm^{-1} wavenumber region. (a): γ-CDEDTA12 hydrogel at *h* = 2.7 (black line), 9.7 (red line), 25.5 (green line); (b): γ-CDEDTA16 hydrogel at *h* = 5.0 (black line), 16.2 (red line), 21.0 (green line); (c) γ-CDEDTA110 hydrogel at *h* = 3.0 (black line), 14.3 (red line), 25.6 (green line).

stretching mode of the functional groups of the cross-linker moiety in the CDNS polymer network [3,4,30]. The spectra of Figure 4 point out a shift towards high wavenumbers and a corresponding reduced intensity of the H-O-H bending vibration of water with increasing hydrogels' hydration level. Interestingly, the opposite trend is observed for the C=O stretching vibration of the polymer, whose maximum tends to shift towards lower wavenumbers and to reduce its intensity at high values of h.

These findings are fully consistent with what already observed for PMA-nanosponge hydrogels [30,47] and explained by considering that the increase of *h* is expected to cause a progressive rearrangement of water molecules in a more cooperative H-bond network. Such configuration, in turn, reinforces the electrostatic environment experienced by the double bonded CO units with the consequent reduction of the overall dipole moment of the CO functional group.

A more quantitative analysis of the changes observed in the hydrogen bond network of confined water molecules as a function of the hydration level *h* was achieved through the decomposition procedure of the O-H stretching band. A well-assessed data handling already reported in literature [48,49] suggests the decomposition of the complex O-H stretching band into single sub-bands which describe classes of O-H oscillators assigned to vibration modes of the water molecules attached or confined in the pores of the CDNS polymeric matrix and involved in different H-bonded transient arrangements with coordination number varying from 0 to 4.

The analysis of the second derivative profiles of the experimental spectra (reported, as example, in the inset of Figure 5a for γ-CDEDTA12 hydrogel at *h* = 5.0) showed four minima approximately corresponding to the maxima of each band component and suggested the presence of four sub-bands with the assigned centre-frequencies, allowing us to overcome the well-known difficulties linked to uniquely fitting IR band profiles [50]. An example of best curve-fitting result is displayed in Figure 5a and 5b for γ-CDEDTA12 hydrogel at *h* = 5.0 and *h* = 16.2, respectively.

The two ω_1 and ω_2 spectral components centred at the lowest wavenumber are assigned, respectively, to the symmetric and asymmetric O-H stretching vibration of water molecules arranged in tetrahedral structures. In such arrangements, both H atoms of each H_2O molecule are involved in strong hydrogen bond. The sub-band ω_3 is ascribed to the non-in-phase O-H stretching mode of H_2O molecules involved in distorted tetrahedral environments connected by "bifurcated" HB. Finally, the highest wavenumber contribution ω_4 takes into account the O-H mode of water molecules whose hydrogen bond network is totally, or at least partially, destroyed [51].

The decomposition procedure mentioned above allowed us to evaluate the relative intensities I_i associated to each ω_i component. These intensities are representative of the population of the different species of water molecules, i.e. water molecules involved in different hydrogen bond patterns. Figure 6 reports, as a specific example, the behaviour, as a function of *h* parameter , of the relative intensities I_i/I_{tot} (i = 1, 2, 3, 4, expressed in %) of the different components of the O-H stretching band obtained in the case of γ-CDEDTA16 hydrogel. In the inset of Figure 6, the *h*-dependence of the centre-frequencies ω_i of each sub-band is also shown.

The wavenumbers ω_i exhibit a slight increase at high values of *h*, suggesting a general enhancement of the strength of the corresponding hydrogen bonds.

The analysis of the I_1-I_4 intensities as a function of *h* reported in Figure 6 indicates that, by increasing the water content in the CDNS hydrogel, a progressively larger number of H_2O molecules will be involved in tetrahedral bulk-like environments (I_1 and I_2) with respect to less coordinated structures (I_3 and I_4). These latter can be thought as "perturbed" hydrogen bond networks of H_2O molecules that are typically affected by the presence of solutes or that are attached to interfaces with suitable receptor sites. It is worth of note a saturation effect revealed by the plateau at the highest *h*-values observed for all the I_i.

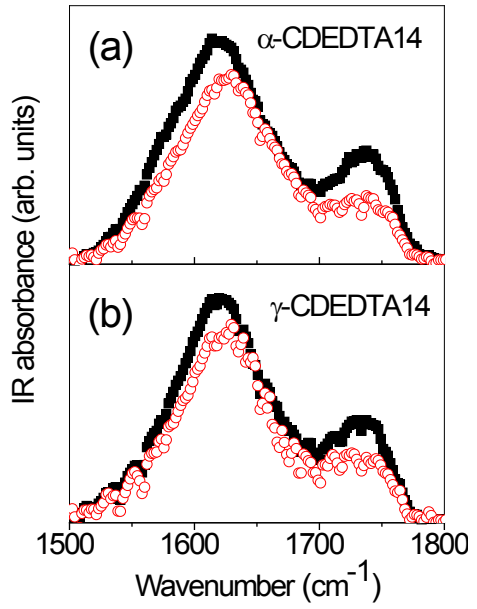

Figure 4: FTIR-ATR spectra in the 1500 ÷ 1800 cm^{-1} region for α- CDEDTA14 (a) and γ-CDEDTA14 (b) hydrogels at h = 3.0 (black closed squares) and h = 21.5 (red open circles), as examples.

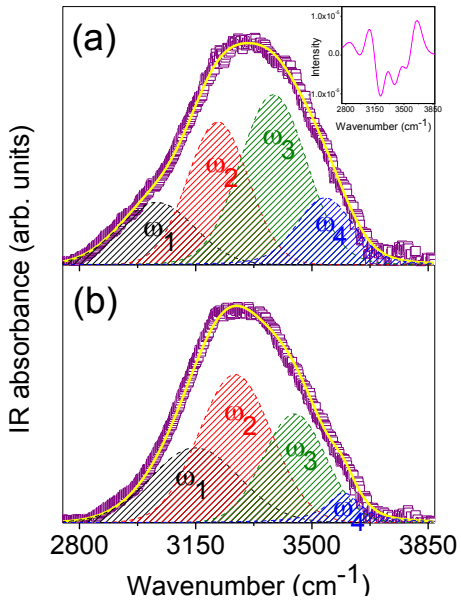

Figure 5: Example of best curve-fitting result of the O-H stretching profile of water for -CDEDTA12 hydrogel at h = 5.0 (a) and h = 16.2 (b). Experimental data (empty squares) are reported together with the total best-fit (continuous line) and the decomposition components (dashed lines). In the inset of the (a) plot, the second derivative profile of the experimental spectrum of γ-CDEDTA12 hydrogel at h = 5.0 is reported as example.

Along with the interest connected to the water molecules dynamics in restricted, porous environment, the data reported above may be useful for spotting into the polymer structure as well. Indeed, in a previous Raman study on water confined in GelSil glass [51] with pores of different diameter, the spectroscopic changes detected in the O-H stretching profile suggested that an enlargement of the pore size gave rise to an enhancement of the population of the bulk-like tetrahedral structures of water molecules. Based on these previous results, we can then hypothesize that the addition of water to CDNS polymers causes an enlargement of the nano-cavities of CDNS up to a certain value compatible with the chemical structure. This hypothesis is supported by very recent small angle neutron scattering results [52], which will be published elsewhere.

Figure 7 displays the evolution, as a function of hydration level h, of the sums of the intensities (I_1+I_2) and (I_3+I_4) obtained for γ-CDEDTA12, γ-CDEDTA16 and γ-CDEDTA110 hydrogels. These quantities account for the population of bulk-like (I_1+I_2) and non-bulk-like (I_3+I_4) water molecules [29], respectively. For all the analysed samples, the experimental data have been fitted by using a logistic sigmoid function (continuous line in Figure 7).

The plots in Figure 7 point out that by increasing the water content in the hydrogel, high-coordinated tetrahedral arrangements of H_2O tend to become favoured with respect to less cooperative patterns. This finding has been explained by considering the saturation of the hydrophilic sites of CDNS that are able to entrap H_2O molecules [27-29] up to a maximum capacity of holding water. As a consequence, any further addition of water will not result in sorption by the porous matrix. Excess water molecules will tend to develop long-distance, highly-interconnected, bulk-like H-bonded arrangements. It is noteworthy that the increasing of high-coordinated tetrahedral arrangements of H_2O at the expenses of the less cooperative HB patterns at high values of the hydration index h has been observed also in other types of CDNS based hydrogels obtained by changing the chemical structure of the cross-linking agent [29], the dimension of the macrocyle [28] and the molar ratio n [27], thus suggesting a general trend.

The behaviour of the complex OH stretching band is also evidenced by the intensity and centre-frequency of the band assigned to H-O-H bending vibration of water reported in Figures 8a and 8b, respectively, for γ-CDEDTA18 hydrogel, as example. A clear decrease of the maximum of the IR absorbance, I_{HOH}, together a shift towards higher wavenumber values of the centre-frequency, ω_{HOH}, of H-O-H bending mode can be clearly observed from the plots of Figure 8.

We remark that the single Gaussian profile shown by the H-O-H

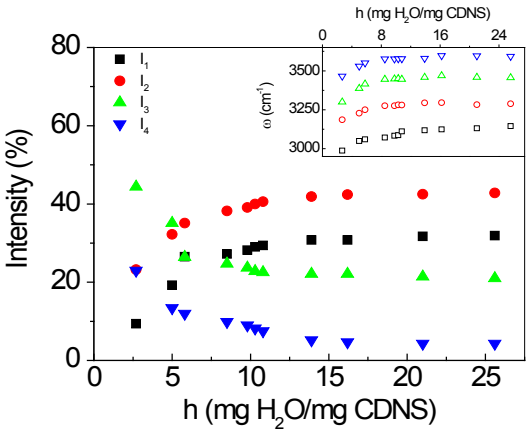

Figure 6: Percentage intensities I_i/I_{tot} (i = 1, 2, 3, 4, expressed in %) of the different spectral components of the O-H stretching band as a function of the hydration level h for γ-CDEDTA16 hydrogel. Inset: h-evolution of the corresponding centre-frequencies ω_i (i = 1, 2, 3, 4, expressed in cm^{-1}).

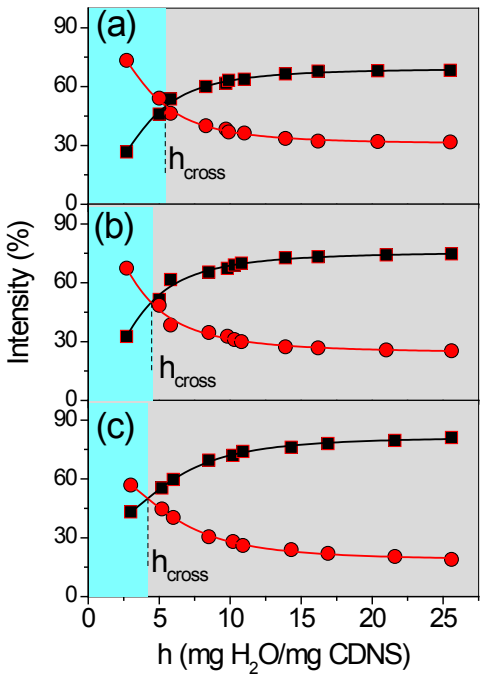

Figure 7: Evolution, as a function of *h*, of the percentage intensities I_1+I_2 (black squares) and I_3+I_4 (red circles) for γ-CDEDTA12 (a), γ-CDEDTA16 (b), and γ-CDEDTA110 (c) hydrogels. For each sample, the characteristic cross-over point h_{cross} is also indicated (see text for details).

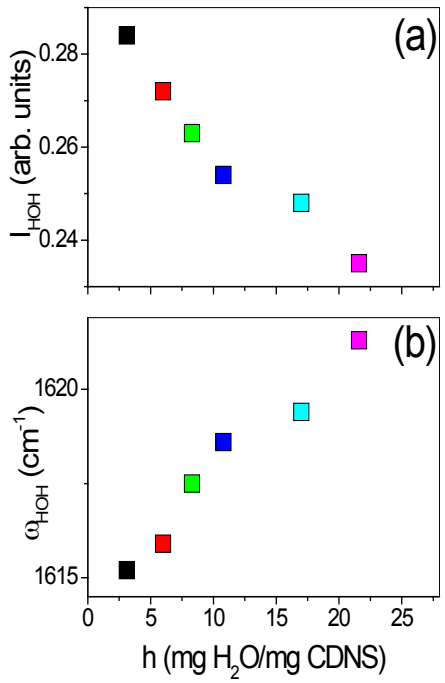

Figure 8: Evolution, as a function of *h*, of the intensity (a) and centre-frequency (b) of the H-O-H bending profile of water for γ-CDEDTA18 hydrogel.

band (Figure 4) indicates that this mode is not appreciably affected by the different patterns of hydrogen bonding of water molecules mentioned before, in contrast to what happens to composite O–H stretching band. As a consequence, the H-O-H bending vibration is easier to interpret than the multiple band highly convoluted water stretching zone.

By using the curves of Figure 7, the cross-over hydration level h_{cross} can be defined and determined: h_{cross} corresponds to the hydration level beyond which the population of bulk-like water molecules becomes larger than the not-bulk-like water. As already discussed for other types of nanosponges hydrogels [27-29], h_{cross} represents the maximum hydration level above which water molecules arrange preferentially in tetrahedral long-range configurations, due to the saturation of the pores of the nanosponge. This point defines two different phases for the system: a rigid gel for $h < h_{cross}$ and a fluid suspension for $h > h_{cross}$ and it can be considered as a quantitative descriptor of the characteristic gel-to-sol transition observed in cyclodextrin nanosponge hydrogels. Likewise, the quantity m = mass ratio = $1/h_{cross}$ can be defined for all the polymers investigated. The mass ratio m gives a quantitative measurement of the water holding capacity at macroscopic scale of CDNS polymer matrix and it corresponds to the gelation point of the system. Thus both m and h_{cross} can be conveniently used as descriptors of the gel-to-sol transition point in CDNS hydrogels.

Now, by making also use of the results of a previously performed FTIR-ATR and Raman investigation on CDNS nanosponges hydrogels obtained by cross-linking with EDTA using β-cyclodextrin as monomer (namely β-CDEDTA1*n*, with $n = 2, 4, 6, 8, 10$), as well as of preliminary data on α-CDEDTA1*n* hydrogels at $n = 2, 6, 10$), an overall picture of the behaviour of mass ratio m as a function of the molar ratio n for these three different types of CDNS hydrogel is proposed in Figure 9a. For α- and β-CDNS a clear trend is detectable, with maximum value corresponding to $n = 6$. For γ-CDNS a negligible dependence on n was observed, for the reasons previously disclosed. In turn, Figure 9b displays the evolution of the measured frequency position of the boson peak ω_{BP} for the same systems in dry state as a function of n.

The comparison of such parameters – ω_{BP} and m – is of particular interest as they describe the system upon different length-scales: the former is related to the elasticity of the polymeric network on a mesoscopic scale, while the latter can be associated to a bulk property of the polymer. A possible correlation of ω_{BP} and m may thus provide a microscopic interpretation to a macroscopic behavior. Moreover, such correlation may provide a more understandable physical interpretation of the Boson peak frequency, so far mainly confined in niche investigation of the physics of matter.

From the inspection of the graphs, it appears evident that both the quantities m and ω_{BP} seem to exhibit, within the experimental error, a similar dependence on the molar ratio n. The molar ratio n influences the degree of reticulation of the polymer during its synthesis. In a previous work [1], an interpretation of the effect of low and high n values on the structure of CDNS was proposed. The cross-linking degree was found to grow with increasing n up to a critical value beyond which, for steric reasons, further cross-linking is inhibited and the cross-linker reagent is attached to the CD as dangling group, thus providing branching of the CD units. The observed trends of both ω_{BP} and m as a function of the molar ratio n, reported in Figure 9, suggest that the elasticity on mesoscopic scale, represented by ω_{BP}, and the water holding capacity on a macroscopic scale, as described by m, undergo the same evolution as a function of the molar ratio n. This opens the possibility to modulate microscopic and macroscopic

properties of this class of materials by operating on a simple process parameter, namely the cross-linker/monomer molar ratio *n*.

In our opinion, this conclusion should deserve attention. Indeed, the elasticity of the network, expressed in terms of elastic constant, can be seen as the key-parameter in determining the swelling properties of the nanosponge.

In this scenario of growing importance of CDNS in pharmaceutical formulations as drug container and/or carrier, a natural evolution of this research would be the clear understanding, at molecular level, of the state of the confined drug inside the polymeric network, especially in the gel state. In this sense, the transport phenomena of a model drug, i.e. Ibuprofen sodium salt (IP) in β-CDEDTA nanosponges were preliminary studied in terms of mean square displacement (MSD) at different observation times [53], highlighting the transition between a subdiffusive to a superdiffusive regime modulated by the polymer structure in a small pH interval (6.5–6.9). The diffusion properties of IP in CDNS can be modulated by suitable polymer synthesis.

Then, the results here reported, at the light of the above considerations, open the possibility to design suitable systems for drug delivery with predictable and desired drug release properties.

Conclusion

The evolution of the stiffness, as derived at mesoscopic level, of the polymeric network obtained by polymerization of α- and γ-CD with the cross-linking agent EDTA is here probed as a function of the CD:EDTA molar ratio *n*. The stiffness is derived by analysing the changes induced by this polymerization process in the so-called Boson Peak (BP) of the resulting cyclodextrin nanosponges, as evidenced by Raman spectroscopy in the low-wavenumber region. For α-CDEDTA1*n* nanosponges, the data revealed, in agreement with previous results, an increase of the hardness of the network with the cross-linking degree up to a critical value of $n = 6$, above which steric effects probably provides branching of CD units. In the case of γ-CDEDTA1*n* nanosponges, the position of the maximum of the BP, ω_{BP}, didn't change significantly, probably because of the enhanced steric hindrance associated to the higher dimension of γ-CD units.

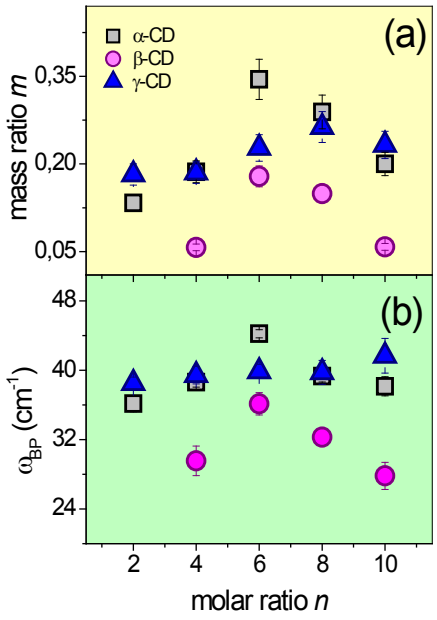

Figure 9: Values of estimated mass ratios $m = 1/h$ (a) and frequency position of the boson peak ω_{BP} (b) for α-CDEDTA1*n* (black squares), β-CDEDTA1*n* (pink circles), and γ-CDEDTA1*n* (blue up triangles) hydrogels as a function of the molar ratio *n*.

After that, CDNS have been progressively hydrated to form hydrogels, and the hydrogen bond scheme developed by water molecules is deeply investigated through FTIR-ATR spectroscopy by looking at the modifications occurring in the O-H stretching and H-O-H bending profiles, with particular regard to the transition from rigid gel to liquid suspension these systems undergo to, described by a key-parameter, the mass ratio *m*, that furnishes a quantitative measurement of the water holding capability of CDNS network, i.e. a macroscopic property of the system.

We found that the elasticity on mesoscopic scale, as described by ω_{BP}, and the swelling ability on a macroscopic scale, as described by *m*, undergo the same evolution as a function of the molar ratio *n*.

Therefore, on the basis of the important information obtained, it should be possible, in principle, to achieve a modulation of the microscopic and macroscopic properties of CDNS by varying the molar ratio *n* during the synthesis process, thus opening the doors to development of suitable stimuli-responsive systems.

Acknowledgement

The authors gratefully acknowledge PRIN 2010-2011 NANOMED prot. 2010 FPTBSH and PRIN 2010-2011 PROxy prot. 2010PFLRJR_005 for financial support.

References

1. Rossi B, Caponi S, Castiglione F, Corezzi S, Fontana A, et al. (2012) Networking properties of cyclodextrin-based cross-linked polymers probed by inelastic light-scattering experiments. J Phys Chem B 116: 5323-5327.
2. Castiglione F, Crupi V, Majolino D, Mele A, Panzeri W, et al. (2013) Vibrational dynamics and hydrogen bond properties of ?-CD nanosponges: a FTIR-ATR, Raman and solid-state NMR spectroscopic study. J Incl Phenom Macrocycl Chem 75: 247-254.
3. Rossi B, Fontana A, Giarola M, Mariotto G, Mele A, et al. (2014) Glass-like dynamics of new cross-linked polymeric systems: Behavior of the Boson peak. J Non Cryst Solids 401: 73-77.
4. Crupi V, Fontana A, Giarola M, Majolino D, Mariotto G, et al. (2013) Connection between the vibrational dynamics and the cross-linking properties in cyclodextrins-based polymers. J Raman Spectrosc 44: 1457-1462.
5. Trotta F, Zanetti M, Cavalli R (2012) Cyclodextrin-based nanosponges as drug carriers. Beilstein J Org Chem 8: 2091-2099.
6. Cavalli R, Akhter AK, Bisazza A, Giustetto P, Trotta F, et al. (2010) Nanosponge formulations as oxygen delivery systems. Int J Pharm 402: 254-257.
7. Swaminathan S, Pastero L, Serpe L, Trotta F, Vavia P, et al. (2010) Cyclodextrin-based nanosponges encapsulating camptothecin: physicochemical characterization, stability and cytotoxicity. Eur J Pharm Biopharm 74: 193-201.
8. Lembo D, Swaminathan S, Donalisio M, Civra A, Pastero L, et al. (2013) Encapsulation of Acyclovir in new carboxylatedcyclodextrin-based nanosponges improves the agent's antiviral efficacy. Int J Pharm 443: 262-272.
9. Chilajwar SV, Pednekar PP, Jadhav KR, Gupta GJ, Kadam VJ (2014) Cyclodextrin-based nanosponges: a propitious platform for enhancing drug delivery. Expert Opin Drug Deliv 11: 111-120.
10. Moya-Ortega MD, Alvarez-Lorenzo C, Concheiro A, Loftsson T (2012) Cyclodextrin-based nanogels for pharmaceutical and biomedical applications. Int J Pharm 428: 152-163.
11. Memisoglu-Bilensoy E, Vural I, Bochot A, Renoir J M, Duchene D, Hincal A A (2005) Tamoxifen citrate loaded amphiphilic beta-cyclodextrin nanoparticles: in vitro characterization and cytotoxicity. J Controlled Release 104: 489-496.

12. Ansari KA, Vavia PR, Trotta F, Cavalli R (2011) Cyclodextrin-based nanosponges for delivery of resveratrol: in vitro characterisation, stability, cytotoxicity and permeation study. AAPS Pharm Sci Tech 12: 279-286.

13. Trotta F, Dianzani C, Caldera F, Mognetti B, Cavalli R (2014) The application of nanosponges to cancer drug delivery. Expert Opin Drug Deliv 11: 931-941.

14. Seglie L, Martina K, Devacchi M, Roggero C, Trotta F, et al. (2011) The effects of 1-MCP in cyclodextrin-based nanosponges to improve the vase life of Dianthus caryophyllus cut flowers. Postharvest Biol Technol 59: 200-205.

15. Li D, Ma M (2000) Nanosponges for water purification. Clean Prod Process 2: 112-116.

16. Liang W, Yang C, Nishijima M, Fukuhara G, Mori T, et al. (2012) Cyclodextrinnano sponge-sensitized enantiodifferentiatingphotoisomerization of cyclooctene and 1,3-cyclooctadiene. Beilstein J Org Chem 8: 1305-1311.

17. Liang W, Yang C, Zhou D, Haneoka H, Nishijima M, et al. (2013) Phase-controlled supramolecularphoto chirogenesis in cyclodextrinnanosponges. Chem Commun (Camb) 49: 3510-3512.

18. Sakurada K, McDonald FM, Shimada F (2008) Regenerative medicine and stem cell based drug discovery. AngewChemInt Ed Engl 47: 5718-5738.

19. Slaughter BV, Khurshid SS, Fisher OZ, Khademhosseini A, Peppas NA (2009) Hydrogels in regenerative medicine. Adv Mater 21: 3307-3329.

20. Gagnon MA, Lafleur M (2009) Self-diffusion and mutual diffusion of small molecules in high-set curdlan hydrogels studied by 31P NMR. J PhysChem B 113: 9084-9091.

21. Brandl F, Kastner F, Gschwind RM, Blunk T, Tessmar J, et al. (2010) Hydrogel-based drug delivery systems: comparison of drug diffusivity and release kinetics. J Control Release 142: 221-228.

22. Lin CC, Boyer PD, Aimetti AA, Anseth KS (2010) Regulating MCP-1 diffusion in affinity hydrogels for enhancing immuno-isolation. J Control Release 142: 384-391.

23. Biondi M, Ungaro F, Quaglia F, Netti PA (2008) Controlled drug delivery in tissue engineering. Adv Drug Deliv Rev 60: 229-242.

24. Peppas NA, Hilt JZ, Khademhosseini A, Langer R (2006) Hydrogels in biology and medicine: From molecular principles to bionanotechnology. Adv Mater 18: 1345-1360.

25. Elisseeff J, McIntosh W, Anseth K, Riley S, Ragan P, et al. (2000) Photoencapsulation of chondrocytes in poly(ethylene oxide)-based semi-interpenetrating networks. J Biomed Mater Res 51: 164-171.

26. Rossi F, Perale G, Masi M (2010) Biological buffered saline solution as solvent in agar-carbomer hydrogel synthesis. Chem Pap 64: 573-578.

27. Crupi V, Majolino D, Mele A, Melone L, Punta C, et al. (2014) Direct evidence of gel-sol transition in cyclodextrin-based hydrogels as revealed by FTIR-ATR spectroscopy. Soft Matter 10: 2320-2326.

28. Castiglione F, Crupi V, Majolino D, Mele A, Melone L, et al. (2014) Gel-sol evolution of cyclodextrin-based nanosponges: role of the macrocycle size. J Incl Phenom Macrocycl Chem 80: 77-83.

29. Crupi V, Fontana A, Majolino D, Mele A, Melone L, et al. (2014) Hydrogen-bond dynamics of water confined in cyclodextrinnanosponges hydrogel. JIncl Phenom Macrocycl Chem 80: 69-75.

30. Crupi V, Majolino D, Mele A, Rossi B, Trotta F, et al. (2013) Modelling the interplay between covalent and physical interactions in cyclodextrin-based hydrogel: effect of water confinement. Soft Matter 9: 6457-6464.

31. Trotta F, Tumiatti W (2003) Patent number WO 03/085002.

32. Trotta F, Tumiatti W, Cavalli R, Roggero CM, Mognetti B, et al. (2009) Patent number WO 09/003656 A1.

33. Maréchal Y (2003) Observing the water molecule in macromolecules and aqueous media using infrared spectrometry. J Mol Struct 648: 27-47.

34. Lewiner L, Klein JP, Puel F, Fevotte G (2001) On-line ATR FTIR measurement of supersaturation during solution crystallization processes. Calibration and applications on three solute/solvent systems. Chem Eng Sci 56: 2069-2084.

35. Hanh BD, Neubert RH, Wartewig S, Christ A, Hentzsch C (2000) Drug penetration as studied by noninvasive methods: fourier transform infrared-attenuated total reflection, fourier transform infrared, and ultraviolet photoacoustic spectroscopy. J Pharm Sci 89: 1106-1113.

36. Chumakov AI, Sergueev I, van Bürck U, Schirmacher W, Asthalter T, et al. (2004) Collective nature of the boson peak and universal transboson dynamics of glasses. Phys Rev Lett 92: 245508.

37. Fabiani E, Fontana A, Buchenau U (2008) Neutron scattering study of the vibrations in vitreous silica and germania. J Chem Phys 128: 244507.

38. Deschamps T, Martinet C, de Ligny D, Bruneel JL, Champagnon B (2011) Correlation between boson peak and anomalous elastic behavior in GeO2 glass: an in situ Raman scattering study under high-pressure. J Chem Phys 134: 234503.

39. Hong L, Begen B, Kisliuk A, Alba-Simionesco C, Novikov VN, et al. (2008) Pressure and density dependence of the boson peak in polymers. Phys Rev B 78: 134201.

40. Crupi V, Fontana A, Giarola M, Longeville S, Majolino D, et al. (2014) Vibrational density of states and elastic properties of cross-linked polymers: combining inelastic light and neutron scattering. J Phys Chem B 118: 624-633.

41. Crupi V, Fontana A, Giarola M, Guella G, Majolino D, et al. (2013) Cyclodextrin-complexation effects on the low-frequency vibrational dynamics of ibuprofen by combined inelastic light e neutron scattering measurements. J Phys Chem B 117: 3917-3926.

42. Caponi S, Corezzi S, Fioretto D, Fontana A, Monaco G, et al. (2009) Raman-scattering measurements of the vibrational density of states of a reactive mixture during polymerization: effect on the boson peak. Phys Rev Lett 102: 027402.

43. Green JL, Lacey AR, Sceats MG (1986) Spectroscopic evidence for spatial correlations of hydrogen bonds in liquid water. J Phys Chem 90: 3959-3964.

44. Langer R, Tirrell DA (2004) Designing materials for biology and medicine. Nature 428: 487-492.

45. Kloxin AM, Kasko AM, Salinas CN, Anseth KS (2009) Photodegradable hydrogels for dynamic tuning of physical and chemical properties. Science 324: 59-63.

46. Brubach JB, Mermet A, Filabozzi A, Gerschel A, Lairez D, et al. (2001) Dependence of water dynamics upon confinement size. J Phys Chem B 105: 430-435.

47. Castiglione F, Crupi V, Majolino D, Mele A, Rossi B, et al. (2013) Vibrational spectroscopy investigation of swelling phenomena in cyclodextrinnano sponges. J Raman Spectrosc, 44: 1463-1469.

48. Cannavà C, Crupi V, Ficarra P, Guardo M, Majolino D, et al. (2008) Physicochemical characterization of coumestrol/β-cyclodextrins inclusion complexes by UV–vis and FTIR-ATR spectroscopies. Vibr. Spectrosc. 48: 172-178.

49. Crupi V, Longo F, Majolino D, Venuti V (2006) Vibrational properties of water molecules adsorbed in different zeolitic frameworks. J. Phys.: Condens. Matter 18: 3563-3580.

50. Lawrence CP, Skinner JL (2003) Ultrafast infrared spectroscopy probes hydrogen bonding dynamics in liquid water. Chem Phys Lett 369: 472-477.

51. Crupi V, Longo F, Majolino D, Venuti V (2007) Raman spectroscopy: Probing dynamics of water molecules confined in nanoporous silica glasses. Eur Phys J Special Topics 141: 61-64.

52. Rossi B, Venuti V, Mele A, Paciaroni A, Crupi V, et al. (2014) Exp. 11776 Exploring the phase diagram of cyclodextrin-based hydrogel. PACE spectrometer at Laboratoire Leon Brillouin (CEA-Saclay).

53. Ferro M, Castiglione F, Punta C, Melone L, Panzeri W2, et al. (2014) Anomalous diffusion of Ibuprofen in cyclodextrinnanosponge hydrogels: an HRMAS NMR study. Beilstein J Org Chem 10: 2715-2723.

Citation: Majolino D, Venuti V, Crupi V, Rossi B, Fontana A et al. (2015) Relationship between Elastic Properties and Gel-to-Sol Transition in Cyclodextrin-Based Hydrogel. Pharm Anal Acta 6: 356. doi:10.4172/2153-2435.1000356